Perturbation evolution started by Richtmyer-Meshkov instability in planar laser targets

Y. Aglitskiy and N. Metzler
Science Applications International Corporation, McLean, Virginia 22150

M. Karasik, V. Serlin, A. L. Velikovich, S. P. Obenschain, A.N. Mostovych, A. J. Schmitt and J. Weaver
Plasma Physics Division, Naval Research Laboratory, Washington, D.C. 20375

J. H. Gardner
Laboratory for Computational Physics and Fluid Dynamics, Naval Research Laboratory, Washington, D.C. 20375

T. Walsh
Schafer Corporation, Livermore, California 94550

Abstract

The first observations of the interaction of the Richtmyer-Meshkov (RM) instability with reflected shock and rarefaction waves in laser-driven targets are reported. The RM growth is started by a shock wave incident upon a rippled interface between low-density foam and solid plastic. Subsequent interaction of secondary rarefaction and/or shock waves arriving from the ablation front and the rear surface of the target with the RM-unstable interface stops the perturbation growth and reverses its direction. The ensuing exponential Rayleigh-Taylor growth thus can sometimes proceed with an inverted phase.

PACS numbers: 52.57.Fg, 47.20.-k, 52.70.La

Report Documentation Page

Form Approved
OMB No. 0704-0188

1. REPORT DATE	2. REPORT TYPE	3. DATES COVERED
2006		**00-00-2006 to 00-00-2006**

4. TITLE AND SUBTITLE	5a. CONTRACT NUMBER
Perturbation evolution started by Richtmyer-Meshkov instability in planar laser targets	5b. GRANT NUMBER
	5c. PROGRAM ELEMENT NUMBER
6. AUTHOR(S)	5d. PROJECT NUMBER
	5e. TASK NUMBER
	5f. WORK UNIT NUMBER
7. PERFORMING ORGANIZATION NAME(S) AND ADDRESS(ES) **Naval Research Laboratory,Plasma Physics Division,4555 Overlook Avenue SW,Washington,DC,20375**	8. PERFORMING ORGANIZATION REPORT NUMBER
9. SPONSORING/MONITORING AGENCY NAME(S) AND ADDRESS(ES)	10. SPONSOR/MONITOR'S ACRONYM(S)
	11. SPONSOR/MONITOR'S REPORT NUMBER(S)

12. DISTRIBUTION/AVAILABILITY STATEMENT
Approved for public release; distribution unlimited

13. SUPPLEMENTARY NOTES
This article appears in Physics of Plasmas and can be found at Aglitskiy et al., Phys. Plasmas 13, 080703 (2006)

14. ABSTRACT
see report

15. SUBJECT TERMS

16. SECURITY CLASSIFICATION OF:			17. LIMITATION OF ABSTRACT	18. NUMBER OF PAGES	19a. NAME OF RESPONSIBLE PERSON
a. REPORT **unclassified**	b. ABSTRACT **unclassified**	c. THIS PAGE **unclassified**	**Same as Report (SAR)**	**17**	

Direct[1] and indirect[2] options of achieving ignition and high energy gain in laser fusion targets both critically depend on our ability to control the Rayleigh-Taylor (RT) perturbation growth in the target associated with its inward acceleration. To predict the degree of target distortion in implosion, and ultimately, the success of ignition on large-scale laser facilities presently under construction,[3] we rely upon numerical simulations. These simulations must accurately model the growth and interaction of the relevant perturbation modes starting from their necessarily very small initial amplitudes. A key issue is the modeling of the early-time transient phase labeled "RT seeding," i. e. formation of the exponentially growing RT eigenmodes from target imperfections, small-scale laser imprint, and large-scale irradiation non-uniformities. Modeling of the RT seeding remains a challenging task for the state-of-the-art hydrocodes used in inertial confinement fusion.[4,5] Therefore code performance needs to be benchmarked against experimental data on the early-time transient processes and RT seeding. Such data started to become available only in the last few years, due to the recent progress in x-ray imaging diagnostics, see Refs. 6-9 and references therein.

As long as the RT seeds contributed by the outer/inner surface and internal target imperfections remain small, and because they are statistically independent, they can be studied in separate experiments. It is appropriate to start with single-mode experiments because they can be diagnosed more easily and the results add useful insight to the seeding process as a whole. In Refs. 6, 7 we reported the first direct observations of the early-time seeding phase caused by the outer – or front, in planar geometry, - surface roughness of the target, the oscillatory process called ablative Richtmyer-Meshkov (RM) instability.[10, 11] The inner – or rear, in planar geometry, - surface roughness of the target

has also been studied as a source of RT seeds. Experiments[7,8] demonstrated the theoretically predicted[12] feedout-triggered areal mass oscillations in a rippled rarefaction wave that is produced in a target rippled on the rear side; see also Ref. 13. These two important cases, however, do not cover all the relevant regimes of the early-time perturbation evolution.

In most target designs, the ablator is not DT ice, but a different material – e. g., solid plastic, DT-wetted or empty CH foam for direct drive,[1] brominated plastic or Be/Cu for indirect drive.[2] Roughness of the material interface between the ablator and the fuel also contributes to the RT seeding. When the shock wave launched at the irradiated surface reaches this embedded interface, its imperfections start growing due to the classical RM instability.[14] The RM growth, which has been studied in a number of laser-driven experiments[15,16] is only the starting phase of the early-time evolution that continues after the secondary rarefaction and/or shock waves arrive at the material interface from the ablation front and the rear surface of the target. Interaction between the RM-unstable interface and these waves, which are all correlated with the perturbations at the interface, gives rise to the oscillatory processes that eventually form the RT seeds.[17] We report here the first direct observations of this interaction in two-layer targets consisting of solid plastic and low-density foam separated with a single-mode sine-wave rippled interface.

Classical light-to-heavy (reflected shock wave) RM instability in the small-amplitude regime is conventionally visualized as a monotonic, asymptotically linear growth of the ripples at the material interface. It is illustrated in Fig. 1(a) by the theoretical curve “interface” showing the contribution of the interfacial ripple amplitude,

$\left(\rho_2^* - \rho_1^*\right) \delta x(t)$, where ρ_1^* and ρ_2^* are the post-shock densities, to the areal mass modulation amplitude, δm, normalized with respect to its initial value, $\delta m_0 = \left(\rho_2 - \rho_1\right) \delta x_0$. Here, $\delta x(t)$ is the ripple amplitude, and $\delta x_0 = \delta x(t = 0)$ is its initial value. This example is constructed using a linear compressible RM theory[10] for the conditions roughly approximating our experiments: foam-to-solid pre-shock density ratio 1:4, perturbation wavelength $\lambda = 30$ μm, a strong incident shock propagating in the foam at $D = 7 \times 10^6$ cm/s hits the interface at $t = 0$, ideal gas equations of state. For the foam, we take $\gamma_1 = 5/3$. Solid plastic is less compressible by the transmitted shock wave – compression ratio of no more than 3 – and therefore a larger value of γ is appropriate;[10, 18] we take here $\gamma_2 = 2$ to match the NRL's CALEOS equation of state for plastic used in our simulations.

Side-on measurements of the interfacial modulation amplitude δx in laser-driven solid targets are difficult, but the total mass modulation amplitude δm is directly measurable by the face-on radiographic diagnostics.[6-9,13] Time history of δm is plotted in Fig. 1(a) as the "total" curve. The areal mass oscillations in the reflected and transmitted shock waves and in the sonic wave fields that the rippled shocks leave behind are superimposed upon the monotonic growth of δm due to the interfacial modulation. As the interfacial growth starts in the positive δm direction, the total mass modulation decreases, forming a minimum of δm, about 2/3 of its initial value, at $t = 0.24$ ns. Lower compressibility of the heavy fluid would make the minima of δm smaller; e. g., for $\gamma_2 = 3$, as in Ref. 18, the first minimum of δm is less than 1/100 of its initial value. This minimum occurs because the negative oscillatory contributions to δm grow faster at

early time than the positive interfacial contribution does. To explain why they are negative, we note that for our light-to-heavy RM configuration, both reflected and transmitted shocks are initially in phase with the original interface perturbation (see the simulated density maps in Fig. 1(c)). Reflected shock front (RS) is concave, and therefore converging. The lateral velocity imposed near the interface at shock refraction drives the shocked foam mass to $y = 0$ from $y = \pm\lambda/2$, hence the corresponding contribution serves to decrease $|\delta m|$. Transmitted shock (TS) is convex, diverging, and the lateral flow drives the shocked CH mass in the opposite direction, thereby increasing $|\delta m|$. Due to lower shock compressibility of the CH, the former contribution prevails, shaping the early-time minimum of $\delta m(t)$, as seen in Fig. 1(c). As both shocks oscillate, not quite in phase, so does their contribution to δm. Figure 1(b) presents the numerically simulated time history of δm for realistic equations of state of foam and plastic, initial interfacial ripple amplitude $\delta x_0 = 1$ μm, normalization and all other conditions being about the same as in Fig. 1(a). The simulated oscillatory growth of δm is in good qualitative agreement with the theoretical prediction of Fig. 1(a).

Transition to an accelerated target provides additional complications. After the target starts to accelerate, the classical RM interfacial growth must evolve into RT. This evolution is not simply a transition from a linear RM growth of δm to a faster, exponential RT growth. Rather, as we demonstrate below, the classical RM growth stops, direction of variation of δm is reversed, and its subsequent RT growth proceeds at inverted phase. This trend is illustrated in Fig. 1(b) by the curve "Nike target," showing the simulated time history $\delta m(t)$ for a two-layer target (120 μm of a 25% solid density CH foam and 20 μm of plastic, initial interfacial ripple amplitude $\delta x_0 = 2.5$ μm,

wavelength $\lambda = 30$ μm) driven by a 4 ns long, 40 TW/cm^2 Nike laser pulse,[6-8,19] on the foam side of the target. For this target, the classical RM growth continues for only 0.6 ns after the incident shock wave hits the foam-plastic interface. Then the RM unstable interface starts interacting with reflected rarefaction waves, first from the CH side then from the foam side, which leads to the RT growth at inverted phase. Even though in this run there is not enough time to invert the phase of δm, the density map in Fig. 1(d) shows some mass redistribution at inverted phase: more high-density-fluid accumulated, and the density contour shape changed form concave to convex, near $y = 0$.

When a shock wave hits a light-to-heavy interface from the light-fluid side, the emerging pressure at the material interface that drives both reflected and transmitted shock waves is higher than the pressure in the incident shock wave, which in our case equals to the pressure that the laser maintains at the ablation front. When the transmitted shock wave reaches the rear surface of the target, and the reflected shock wave reaches the ablation front, the shocked fluid decompresses – to zero pressure at the target rear, and to the laser-supported pressure at the ablation front. Reflected rarefaction waves propagate back to the RM-unstable material interface from both directions. As soon as one of the rarefaction waves reaches it, the classical RM growth stops. Whether this wave comes from the heavy fluid (as is typical for our targets) or from the light fluid side, the light fluid decompresses faster because of its higher speed of sound. Higher pressure in the spikes of heavy fluid drives it laterally into the bubbles of light fluid, thus changing the direction of variation of δm, as shown in Fig. 1(b). Inertia of this motion shapes the areal mass perturbation profile with inverted phase, which is later exponentially amplified by the RT instability.

We observed this process using the same experimental setting as in.[6-8] Our experiments were performed with the Nike KrF laser,[19] $\lambda_L = 248$ nm. The 4 ns long laser pulse, with or without a ~5%, 3 ns foot was focused to a spot 750 μm in diameter, producing intensity up to 50 TW/cm^2. The time-averaged rms spatial variation for the 37 Nike beams overlapping at the focal spot is below 0.3%; hence the RM-RT related evolution is not obscured by the laser imprint effects.

The diagnostic setup, same as in Refs. 6-8, is the Nike monochromatic x-ray imaging system coupled to an x-ray streak camera. The He-like resonance line of Si, $h\nu = 1.86$ keV, selected by a spherically curved quartz crystal from the radiation of a silicon backlighter, illuminated the main target for ~5 ns. The monochromatic image of the target was projected on the entrance slit of the x-ray streak camera with positioning accuracy of 30 μm. We registered face-on image of the target evolving continuously in time, with spatial resolution in one relevant direction and time resolution of ~170 ps, which allowed us to directly observe the time evolution of δm for relevant Fourier modes. The targets, manufactured for our experiments by Schafer Corporation, featured a single-mode, two-dimensional sine-wave rippled interface separating low-density resorcinol formaldehyde foam from solid plastic. This represents an important progress in target manufacturing – similar targets used in earlier laser RM experiments,[16] consisted of rippled plastic layers that were in contact with planar foam layers only at peaks. Typical parameters of our targets are: ripple wavelength $\lambda = 30$ μm, ripple amplitude $\delta x_0 = 2.5$ μm, 23 μm layer of solid plastic, $\rho_2 = 1.07$ g/cm^3, and 130 μm foam layer, $\rho_1 = (0.2 - 0.3) \times \rho_2$. The targets could be irradiated from either side, triggering light-to-heavy, as in Fig. 1, or heavy-to-light classical RM instability at the foam-plastic interface.

Figure 2 compares the numerical predictions and the experimental results for the targets irradiated from the foam side by Nike pulses without (a) and with foot (b). Here and below $t = 0$ corresponds to the half-rise of the main pulse, and the mode amplitude shown is the absolute value $|\delta m(t)|$ for the dominant Fourier divided by ρ_2. The simulations predict almost constant velocity of the material interface before the onset of acceleration marked by the star, when the RT growth starts. When the laser pulse has a foot, Fig. 2(b), the classical RM growth of δm is predicted to stop earlier, and to peak at lower amplitude. This happens because with the foam pre-compressed by the foot, the classical RM growth phase becomes shorter, the interaction of the RM-unstable interface with the secondary rippled rarefaction waves occurs earlier, and the lateral mass flow triggered by it continues long enough to invert the phase of δm and drive the RT growth with the inverted phase. This is exactly what we observe in the experiment; see Fig. 2(b). The peak values of $|\delta m|$ are observed to exceed δm_0 by factors of 3.2 and 4.3, for Nike pulses with and without foot, respectively. The corresponding simulated growth factors for these two cases are 3.6 and 6.0.

Our simulations predict a phase reversal of δm before the end of the main pulse for the Nike pulse with a foot: The mass modulation amplitude passes through zero and continues to grow in the negative direction, accumulating more areal mass where there was less of it initially. Observations confirm this phase reversal, as illustrated by Fig. 2(c). It presents the lineouts of the streak records taken at the moments $t = 3$ and 4 ns indicated by stars on the "foot" $|\delta m(t)|$ trace in Fig. 2(b). We see that as $|\delta m|$ passes through its minimum value below the noise level, its phase changes by $180°$, with valleys of areal mass observed at 4 ns at exactly the same places where the peaks were at 3 ns.

The early-time minimum of $\delta m(t)$ predicted by the theory and simulations (Figs. 1, 2) is not resolved with our signal-to-noise ratio at low amplitudes, even though the observed time histories of δm shown in Fig. 2 do not contradict its presence.

When the target is reversed and the shock wave in solid plastic hits the plastic-foam interface, it triggers the heavy-to-light classical RM instability. In contrast with the light-to-heavy case of Fig. 1, the amplitude δm is predicted to rapidly change sign and grow monotonically in the negative direction, as observed in Refs. 15,16 and discussed in detail in Ref. 12. Figure 3 shows the numerical predictions and experimental results for a similar plastic-foam target irradiated from the plastic side. We do not see a big difference between Figs. 2 and 3 because the time histories shown there are not dominated by either case of the classical RM instability, but rather by the interaction of the secondary rarefaction and/or shock waves arriving from the ablation front and the rear surface of the target with the RM-unstable interface. In Fig. 3 the time available for the classical RM growth is very short, about 0.2 ns, because of the small thickness of the heavy plastic layer. After the shock passes the interface, a reflected rarefaction wave starts propagating into the shock-compressed solid plastic, and a transmitted shock wave - into the unperturbed foam. When the reflected rarefaction wave reaches the ablation front, where a higher pressure is maintained, a so-called adjustment shock is reflected from it, propagating in the heavy fluid back to the RM unstable interface. Re-shock of the interface reverses the direction of the growth of δm, from negative to positive. This growth in the positive direction continues until the adjustment shock reaches the transmitted shock front and a rarefaction wave reflected from it comes back to the interface, once again reversing the direction of variation of δm as described above (see

Figs. 1 and 2). For a laser pulse with a foot, the incident shock wave in plastic is slower, there is more time available for the classical heavy-to-light RM growth in the negative direction, and larger amplitude of interfacial modulation is reached by the time when the interface is re-shocked. Since the shock wave transmitted into the foam is also slower, the interval between the re-shock and the arrival of the rarefaction wave reflected from the rear surface to the material interface is longer, allowing more time for the RM growth in the positive direction after the re-shock. Therefore the peak of $|\delta m|$ is predicted to be higher for the pulse with a foot, in contrast with the situation of Fig. 2 when the target is irradiated from the low-density foam side. Experimental data demonstrate that this is indeed the case: a higher peak is observed for the Nike pulse with a foot, Fig. 3(b). Ablation front starts accelerating shortly before the end of the pulse, hence no time is left for the RT growth. Indeed, no late-time phase reversal is observed for either case, as predicted by the simulations.

To summarize, we have observed for the first time the oscillatory transient processes responsible for the evolution of perturbation growth triggered by the classical RM instability at a shocked material interface in a laser target through the onset of the RT growth when the target starts to accelerate. The observed evolution of perturbations is in agreement with our theory and simulations.

The authors are grateful to the Nike Laser Crew for excellent technical support. This work was sponsored by the U.S. Department of Energy, NNSA Defense Programs.

References

[1] S. E. Bodner, D. G. Colombant, J. H. Gardner, R. H. Lehmberg, S. P. Obenschain, L. Phillips, A. J. Schmitt, J. D. Sethian, R. L. McCrory, W. Seka, C. P. Verdon, J. P. Knauer, Bedros B. Afeyan and Howard T. Powell, Phys. Plasmas **5**, 1901 (1998); S. E. Bodner, D. G. Colombant, A. J. Schmitt, and M. Klapisch, Phys. Plasmas **7**, 2298 (2000); S. E. Bodner, D. G. Colombant, A. J. Schmitt, J. H. Gardner, R. H. Lehmberg, S. P. Obenschain, Fusion Engineering and Design **60**, 93(2002).

[2] J. D. Lindl, P. Amendt, R. L. Berger, S. G. Glendinning, S. H. Glenzer, S. W. Haan, R. L. Kauffman, O. L. Landen, and L. J. Suter, Phys. Plasmas **11**, 339 (2004).

[3] E. I. Moses and C. R. Wuest, Fusion Science and Technology **47**, 314 (2005); C. Cavailler, N. Fleurot, T. Lonjaret and J.-M. Di-Nicola, Plasma Phys. Contr. Fusion **46**, B135 (2004).

[4] A. J. Schmitt, D. Colombant, A. L. Velikovich, S. Zalesak, J. H. Gardner, D. Fyfe, and N. Metzler, Phys. Plasmas **11**, 2716 (2004).

[5] S. T. Zalesak, A. J. Schmitt, J. H. Gardner, and A. L. Velikovich, Phys. Plasmas **12**, 056311 (2005).

[6] Y. Aglitskiy, A. L. Velikovich, M. Karasik, V. Serlin, C. J. Pawley, A. J. Schmitt, S. P. Obenschain, A. N. Mostovych, J. H. Gardner, and N. Metzler, Phys. Rev. Lett. **87**, 265001 (2001).

[7] Y. Aglitskiy, A. L. Velikovich, M. Karasik, V. Serlin, C. J. Pawley, A. J. Schmitt, S. P. Obenschain, A. N. Mostovych, J. H. Gardner, and N. Metzler, Phys. Plasmas **9**, 2264 (2002).

[8] Y. Aglitskiy, A. L. Velikovich, M. Karasik, V. Serlin, C. J. Pawley, A. J. Schmitt, S. P. Obenschain, A. N. Mostovych, J. H. Gardner, and N. Metzler, Phys. Rev. Lett. **87**, 265002 (2001).

[9] O. V. Gotchev, P. A. Jaanimagi, J. P. Knauer, F. J. Marshall, and D. D. Meyerhofer, Rev. Sci. Instrum. **75**, 4063 (2004).

[10] A. L. Velikovich, J. P. Dahlburg, J. H. Gardner, and R. J. Taylor, Phys. Plasmas **5**, 1491 (1998).

[11] V. N. Goncharov, Phys. Rev. Lett. **82**, 2091 (1999).

[12] A. L. Velikovich, A. J. Schmitt, J. H. Gardner, and N. Metzler, Phys. Plasmas **8**, 592 (2001).

[13] D. P. Smitherman, R. E. Chrien, N. M. Hoffman and G. R. Magelssen, Phys. Plasmas **6**, 932 (1999); K. Shigemori, M. Nakai, H. Azechi, K. Nishihara, R. Ishizaki, T. Nagaya, H. Nagamoto and K. Mima, Phys. Rev. Lett. **84**, 5331 (2000).

[14] R. D. Richtmyer, Commun. Pure Appl. Math. **13**, 297 (1960); E. E. Meshkov, Fluid Dyn. **4**, No. 5, 101 (1969).

[15] G. Dimonte and B. Remington, Phys. Rev. Lett. **70**, 1806 (1993).

[16] S. G. Glendinning, J. Bolstad, D. G. Braun, M. J. Edwards, W. W. Hsing, B. F. Lasinski, H. Louis, A. Miles, J. Moreno, T. A. Peyser, B. A. Remington, H. F. Robey, E. J. Turano, C. P. Verdon, and Y. Zhou, Phys. Plasmas **10**, 1931 (2003).

[17] N. Metzler, , A. L. Velikovich, A. J. Schmitt, M. Karasik, V. Serlin, A. N. Mostovych, S. P. Obenschain, J. H. Gardner, and Y. Aglitskiy, Phys. Plasmas **10**, 1897 (2003).

[18] R. Ishizaki and K. Nishihara, Phys. Rev. Lett. **78**, 1920 (1997).

[19] S. P. Obenschain, S. E. Bodner, D. Colombant, K. Gerber, R. H. Lehmberg, E. A. McLean, A. N. Mostovych, M. S. Pronko, C. J. Pawley, A. J. Schmitt, J. D. Sethian, V. Serlin, J. A. Stamper, C. A. Sullivan, J. P. Dahlburg, J. H. Gardner, Y. Chan, A. V. Deniz, J. Hardgrove, T. Lehecka, and M. Klapisch, Phys. Plasmas **3**, 2098 (1996).

Figure captions

Figure 1 (Color). (a) Theoretical time histories of δm for classical light-to-heavy RM instability: total δm (red line), and contribution to it due to the interfacial perturbation (blue line). (b) Simulated $\delta m(t)$ for a shock-interface interaction in an unbounded medium (solid line) and in a finite-thickness Nike target (dashed lines). (c) Simulated density map for the classical RM case at the moment marked by the solid circle in (b); TS, RS and MI denote transmitted and reflected shock fronts and material interface, respectively. (d) Same for the Nike target at the moment marked by the empty circle in (b).

Figure 2. Simulated (black) and measured (gray lines) $|\delta m(t)|$ for a target irradiated from the foam side by Nike pulses without (a) and with foot (b). Stars in (a), (b) indicate the onset of acceleration. (c) Lineouts of the streak records at 3 and 4 ns showing a phase reversal of areal mass modulation.

Figure 3. Simulated (black) and measured (gray lines) $|\delta m(t)|$ for a target irradiated from the plastic side by Nike pulses without (a) and with foot (b). Stars in (a), (b) indicate the onset of acceleration. Gray solid and dashed lineouts represent two shots taken consequently in order to cover whole laser pulse without foot.

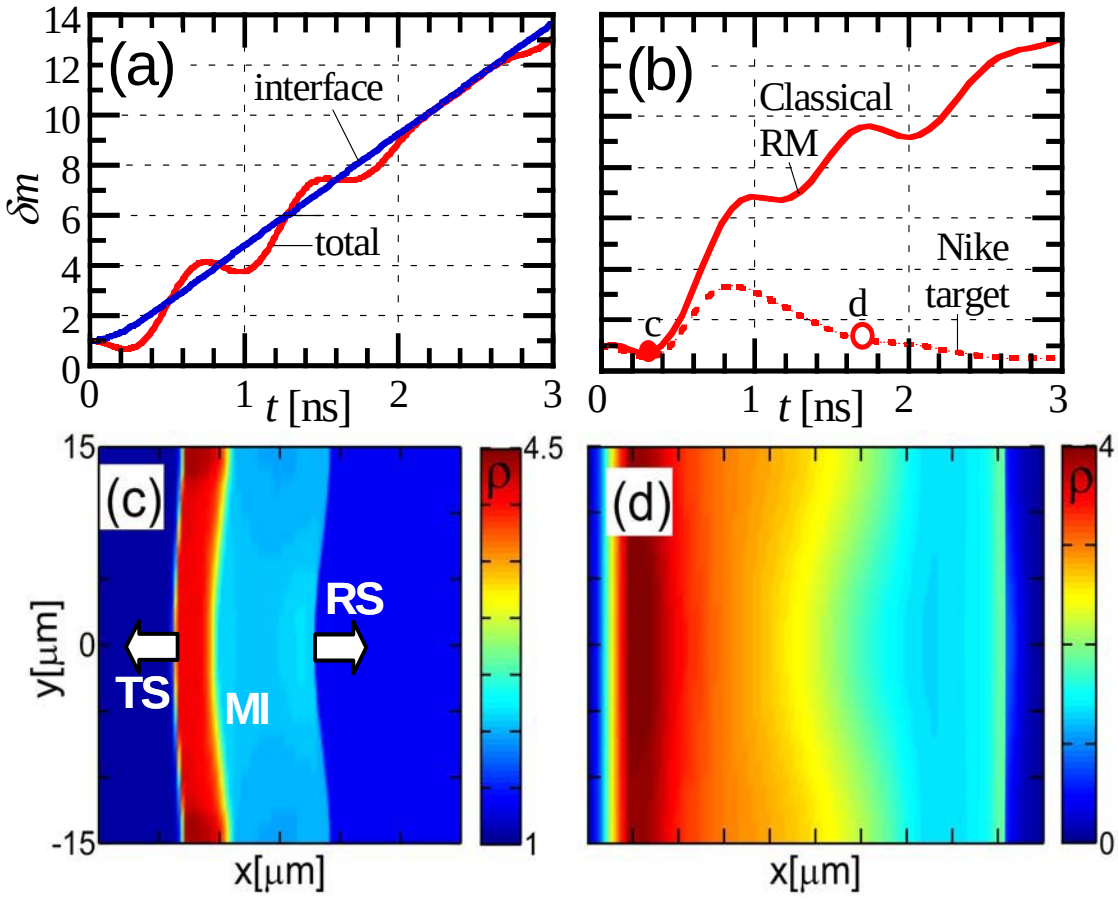

Figure 1 (Color). (a) Theoretical time histories of δm for classical light-to-heavy RM instability: total δm (red line), and contribution to it due to the interfacial perturbation (blue line). (b) Simulated $\delta m(t)$ for a shock-interface interaction in an unbounded medium (solid line) and in a finite-thickness Nike target (dashed lines). (c) Simulated density map for the classical RM case at the moment marked by the solid circle in (b); TS, RS and MI denote transmitted and reflected shock fronts and material interface, respectively. (d) Same for the Nike target at the moment marked by the empty circle in (b).

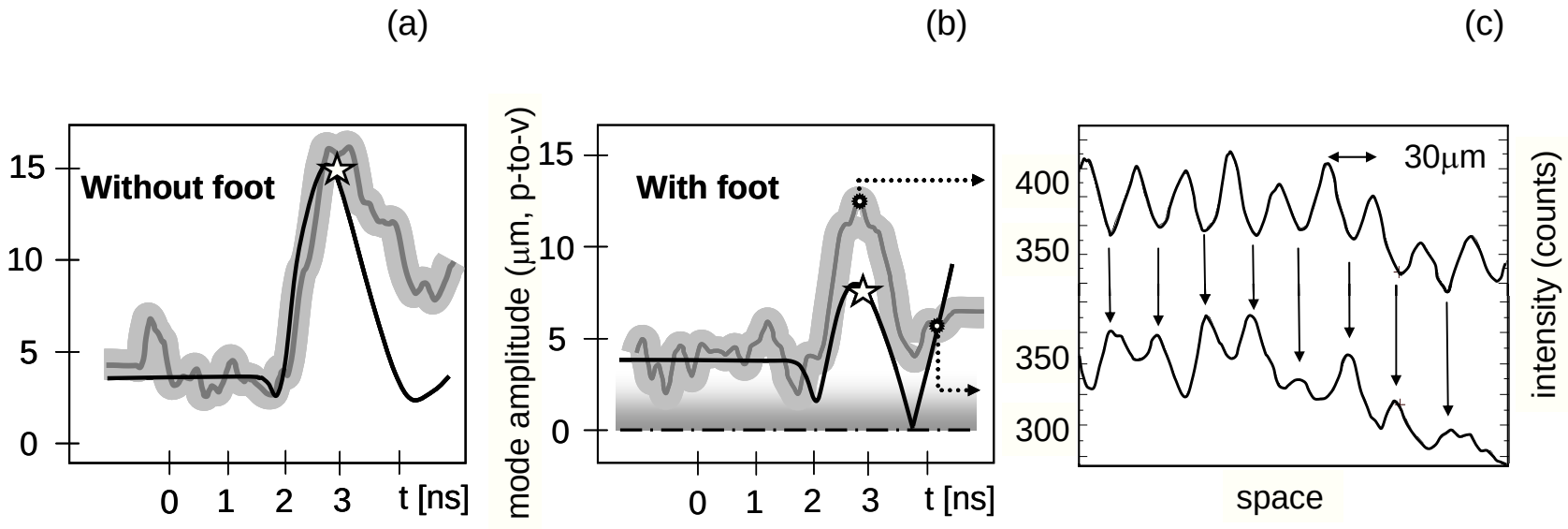

Figure 2. Simulated (black) and measured (gray lines) $|\delta m(t)|$ for a target irradiated from the foam side by Nike pulses without (a) and with foot (b). Stars in (a), (b) indicate the onset of acceleration. (c) Lineouts of the streak records at 3 and 4 ns showing a phase reversal of areal mass modulation. The thickness of the shaded area approximately corresponds to the experimental uncertainty of the Fourier amplitude measurement near zero.

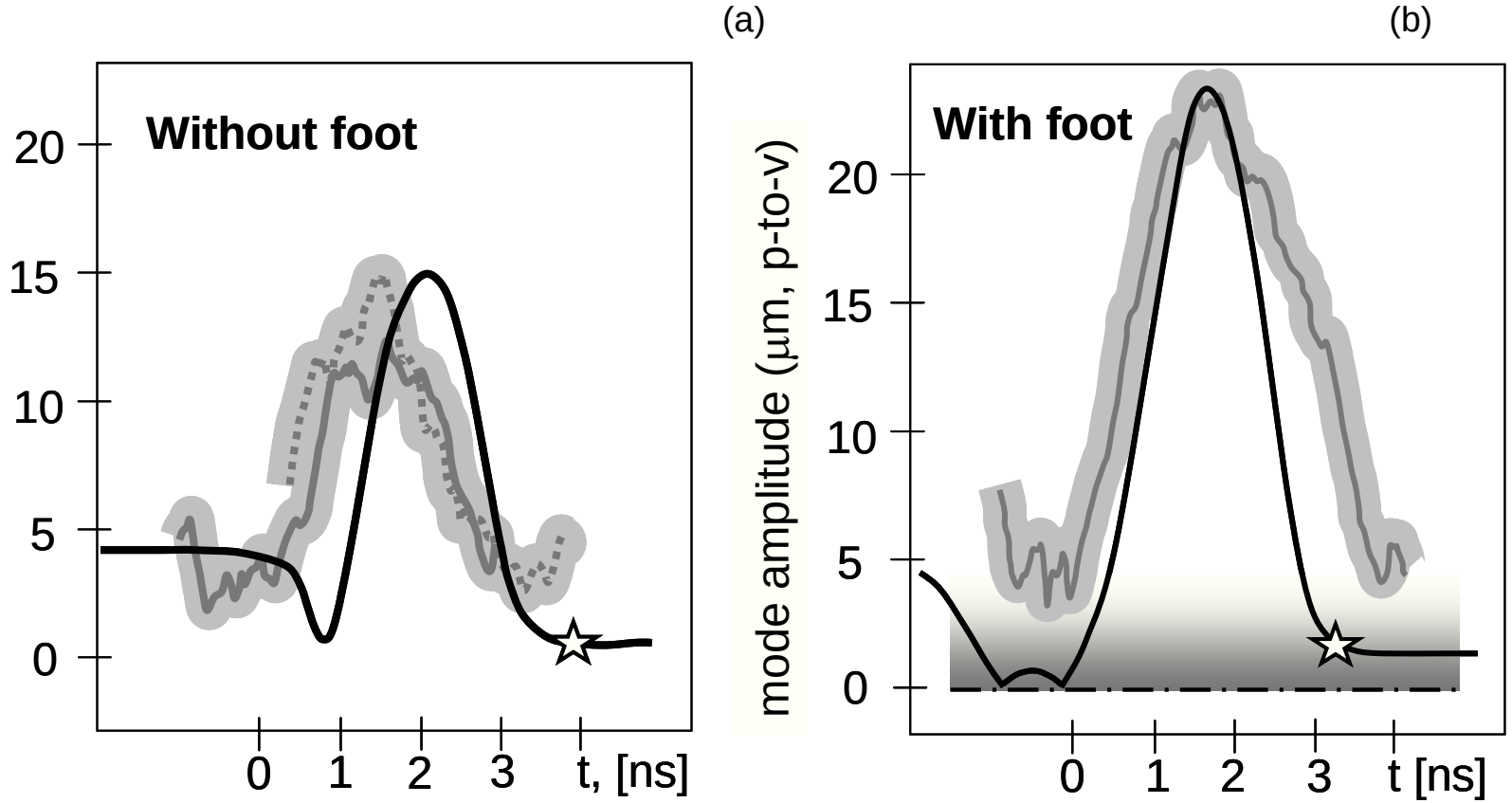

Figure 3. Simulated (black) and measured (gray lines) $|\delta m(t)|$ for a target irradiated from the plastic side by Nike pulses without (a) and with foot (b). Stars indicate the onset of acceleration. Gray solid and dashed lineouts represent two shots taken consequently in order to cover whole laser pulse without foot. The thickness of the shaded area approximately corresponds to the experimental uncertainty of the Fourier amplitude measurement near zero.